Targeting myostatin/activin A protects against skeletal muscle and bone loss during spaceflight

Se-Jin Lee[a,b,1], Adam Lehar[a], Jessica U. Meir[c], Christina Koch[c], Andrew Morgan[c], Lara E. Warren[d], Renata Rydzik[e], Daniel W. Youngstrom[e], Harshpreet Chandok[a], Joshy George[a], Joseph Gogain[f], Michael Michaud[a], Thomas A. Stoklasek[a], Yewei Liu[a], and Emily L. Germain-Lee[g,h]

[a]The Jackson Laboratory for Genomic Medicine, Farmington, CT 06032; [b]Department of Genetics and Genome Sciences, University of Connecticut School of Medicine, Farmington, CT 06030; [c]The National Aeronautics and Space Administration, NASA Johnson Space Center, Houston, TX 77058; [d]Center for the Advancement of Science in Space, Houston, TX 77058; [e]Department of Orthopaedic Surgery, University of Connecticut School of Medicine, Farmington, CT 06030; [f]SomaLogic, Inc., Boulder, CO 80301; [g]Department of Pediatrics, University of Connecticut School of Medicine, Farmington, CT 06030; and [h]Connecticut Children's Center for Rare Bone Disorders, Farmington, CT 06032

Contributed by Se-Jin Lee, August 4, 2020 (sent for review July 14, 2020; reviewed by Shalender Bhasin and Paul Gregorevic)

Among the physiological consequences of extended spaceflight are loss of skeletal muscle and bone mass. One signaling pathway that plays an important role in maintaining muscle and bone homeostasis is that regulated by the secreted signaling proteins, myostatin (MSTN) and activin A. Here, we used both genetic and pharmacological approaches to investigate the effect of targeting MSTN/activin A signaling in mice that were sent to the International Space Station. *Wild type* mice lost significant muscle and bone mass during the 33 d spent in microgravity. Muscle weights of *Mstn* $^{-/-}$ mice, which are about twice those of *wild type* mice, were largely maintained during spaceflight. Systemic inhibition of MSTN/activin A signaling using a soluble form of the activin type IIB receptor (ACVR2B), which can bind each of these ligands, led to dramatic increases in both muscle and bone mass, with effects being comparable in ground and flight mice. Exposure to microgravity and treatment with the soluble receptor each led to alterations in numerous signaling pathways, which were reflected in changes in levels of key signaling components in the blood as well as their RNA expression levels in muscle and bone. These findings have implications for therapeutic strategies to combat the concomitant muscle and bone loss occurring in people afflicted with disuse atrophy on Earth as well as in astronauts in space, especially during prolonged missions.

myostatin | activin | skeletal muscle | bone | microgravity

Myostatin (MSTN, GDF-8) is a transforming growth factor-β (TGF-β) superfamily member that normally acts to limit skeletal muscle mass (1, 2). Mice carrying a targeted deletion of the *Mstn* gene exhibit dramatic muscle growth, with individual muscles weighing about twice as much as those of *wild type* mice (2). The function of MSTN has been strongly conserved through evolution, as targeted or naturally occurring mutations in cattle (3–5), sheep (6), dogs (7), rabbits (8), rats (9), swine (10), and goats (11) have all been shown to lead to increased muscling. Moreover, a heavily muscled boy was found to carry a mutation in a splice site in the *MSTN* gene, showing that MSTN plays a similar role in humans as well (12). A number of pharmaceutical and biotechnology companies have developed MSTN inhibitors that have been tested in human clinical trials for a wide range of conditions characterized by muscle loss, although none of these trials have yet led to drug approval for clinical use in any disease setting.

The function of MSTN in muscle is at least partially redundant with that of another TGF-β family member, activin A (13–16). Like other TGF-β family members, both MSTN and activin A signal through a complex of type II and type I receptors. Signaling is initiated by binding of these ligands to the activin type II receptors, ACVR2 and ACVR2B (17). A decoy receptor (ACVR2B/Fc) consisting of the extracellular, ligand-binding domain of ACVR2B fused to an immunoglobulin Fc domain has been shown to be a potent inhibitor of MSTN and activin A signaling and, as a result, can induce significant muscle growth when given systemically to *wild type* mice (13). Indeed, by blocking both ligands, this decoy receptor can induce significantly more muscle growth than other MSTN inhibitors, and at high doses, ACVR2B/Fc can induce over 50% muscle growth in just 2 wk.

Moreover, because this decoy receptor can block not only MSTN but also activin A, systemic administration of ACVR2B/Fc can also lead to significant increases in bone density (18–20). The dual ability of ACVR2B/Fc to promote muscle growth and to increase bone density has suggested the possibility that this therapeutic strategy may be particularly useful to combat simultaneously comorbid muscle and bone loss, and indeed, this strategy has been shown to be effective in a mouse model of osteogenesis imperfecta, which is characterized by both muscle atrophy and bone fragility (21, 22).

Another setting in which both muscle and bone loss can lead to significant disability is disuse atrophy, which occurs not only during aging and in individuals of all ages who are bedridden or wheelchair-bound from illness but also in astronauts during prolonged space travel. Although advances in exercise devices and nutrition have significantly attenuated the bone mineral density losses observed during prolonged missions on vehicles

Significance

Among the major health challenges for astronauts during prolonged space travel are loss of muscle mass and loss of bone mass. Here, we investigated the effects of targeting the signaling pathway mediated by the secreted signaling molecules, myostatin and activin A, in mice sent to the International Space Station. We show that targeting this signaling pathway has significant beneficial effects in protecting against both muscle and bone loss in microgravity, suggesting that this strategy may be effective in preventing or treating muscle and bone loss not only in astronauts on prolonged missions but also in people with disuse atrophy on Earth, such as in older adults or in individuals who are bedridden or wheelchair-bound from illness.

Author contributions: S.-J.L. and E.L.G.-L. designed research; S.-J.L., A.L., J.U.M., C.K., A.M., R.R., M.M., T.A.S., Y.L., and E.L.G.-L. performed research; S.-J.L., A.L., D.W.Y., H.C., J. George, J. Gogain, and E.L.G.-L. analyzed data; S.-J.L., A.L., J.U.M., L.E.W., D.W.Y., H.C., J. George, J. Gogain, M.M., Y.L., and E.L.G.-L. wrote the paper; and S.-J.L., A.L., L.E.W., and E.L.G.-L. provided project administration.

Reviewers: S.B., Brigham and Women's Hospital; and P.G., University of Melbourne.

The authors declare no competing interest.

[1]To whom correspondence may be addressed. Email: sejlee@uchc.edu.

This article contains supporting information online at https://www.pnas.org/lookup/suppl/doi:10.1073/pnas.2014716117/-/DCSupplemental.

First published September 8, 2020.

like the International Space Station (ISS) (23, 24), future exploration missions to destinations like Mars will be significantly longer (~3 y) and impose mass constraints that will not allow for the same, highly effective exercise equipment. Thus, therapeutic strategies, such as those related to MSTN/activin A signaling, may be critical to maintain astronaut health in such missions. Here, we describe the results of a study, named Rodent Research-19 or "Sending Mighty Mice to Space," in which we tested whether loss of MSTN/activin A signaling can prevent or mitigate muscle and/or bone loss in mice sent to the ISS. We show that inhibition of myostatin/activin A signaling can have a significant protective effect against microgravity-induced muscle and bone loss.

Results and Discussion

A total of 40 mice were launched on SpaceX-19 from the NASA Kennedy Space Center (KSC) on December 5, 2019 and were transferred to the ISS on December 10. The mice remained onboard ISS until the departure of SpaceX on January 7, 2020 and were delivered live to Explora Biolabs ~32 h after splashdown in the Pacific Ocean (live animal return, LAR). The 40 mice comprised five groups of eight female mice each, and a timeline for the sequence of experimental interventions is shown in Fig. 1*A*. Three groups comprised untreated *wild type* mice, one group comprised *wild type* mice that were treated with ACVR2B/Fc, and one group comprised *Mstn* $^{-/-}$ mice. All but 16 uninjected *wild type* mice were euthanized for analysis within the first 8 h after LAR. The remaining 16 mice were maintained live at Explora for an additional 14 d after LAR, with eight receiving two injections of ACVR2B/Fc. In addition to this cohort of 40 flight mice, a cohort of 24 ground control mice was maintained at KSC on a 2 d delay relative to the flight mice so that the environmental conditions recorded for the flight mice aboard the ISS could be reproduced for the ground mice. These ground control mice (eight uninjected *wild type*, eight ACVR2B/Fc-injected *wild type*, and eight *Mstn* $^{-/-}$) were sent by ground transport to Explora on the day corresponding to LAR.

Exposure of *wild type* mice to microgravity for 33 d led to significant muscle loss, with lean body mass being lower by 9% and weights of pectoralis, triceps, quadriceps, gastrocnemius/plantaris, and soleus muscles being lower by 8%, 8%, 15%, 14%, and 18%, respectively, compared to *wild type* mice maintained on Earth (Fig. 1*B*). As described previously (2), ground *Mstn* $^{-/-}$ mice had an approximate doubling of muscle mass throughout the body compared to ground *wild type* mice (Fig. 1*B*). These differences were substantially maintained in *Mstn* $^{-/-}$ mice that returned to Earth after being subjected to microgravity. There was a trend toward lower values in flight versus ground *Mstn* $^{-/-}$ mice, with the absolute differences being similar to those seen in flight versus ground *wild type* mice; these differences, however, were significantly smaller in *Mstn* $^{-/-}$ mice as a percentage of starting muscle mass (Fig. 1*C*) and were not statistically significant. Regardless of whether these differences are meaningful, these data show that the enhanced muscling due to loss of MSTN is largely (if not entirely) maintained following exposure to microgravity.

We observed a similar effect in mice in which we blocked MSTN/activin A signaling by administering the ACVR2B/Fc decoy receptor. We showed previously that treatment with ACVR2B/Fc can induce rapid muscle growth (13), and indeed, the decoy receptor increased lean body mass in ground mice by 11% in just 12 d (Fig. 1*D*). The ability of ACVR2B/Fc to promote muscle growth in microgravity was clearly evident in comparing the data between the two in-flight dual-energy X-ray absorptiometer (DXA) scans on days L+6 and L+28. Lean body

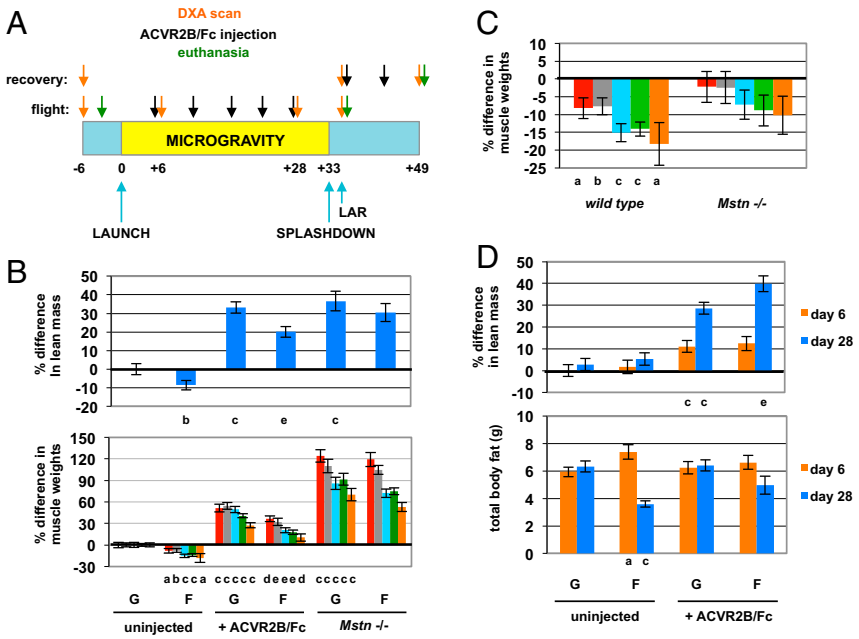

Fig. 1. Mitigation of skeletal muscle loss in microgravity by targeting myostatin/activin A signaling. (*A*) Schematic showing the timeline of interventions and procedures. The timings of DXA scans, ACVR2B/Fc injections, and euthanasia are shown by orange, black, and green arrows, respectively. The timeline for mice in groups 1 to 3 is labeled as "flight," and the timeline for mice in groups 4 to 5 is labeled as "recovery" (see *Methods* for group designations). (*B*) Effect of microgravity on lean body mass (*Upper*) and muscle weights (*Lower*) expressed as percent differences relative to uninjected ground mice at LAR. Bars in *Lower* represent pectoralis (red), triceps (gray), quadriceps (blue), gastrocnemius/plantaris (green), and soleus (orange) muscles. G, ground control mice; F, flight mice. (*C*) Percent differences in muscle weights in flight relative to corresponding ground mice at LAR. Bars represent muscles as described in *B*. None of the differences seen in *Mstn* $^{-/-}$ mice were statistically significant. (*D*) Changes in lean body mass (*Upper*) and total body fat (*Lower*) between the two in-flight DXA scans on days L+6 and L+28. In the *Upper*, percent differences in lean mass were calculated relative to ground mice at day L+6 (i.e., all numbers were normalized to ground mice at day +6, which was set to zero).[a] $P < 0.05$, [b] $P < 0.01$, [c] $P < 0.001$ versus uninjected ground mice; [d] $P < 0.01$, [e] $P < 0.001$ versus ACVR2B/Fc-injected ground mice.

mass in ACVR2B/Fc-treated flight mice increased by 27% over these 22 d, which was even significantly more than the increases seen in ground mice (18%). Comparison of data from the two in-flight DXA scans also revealed a significant reduction in overall body fat as a result of being subjected to microgravity (Fig. 1*D*), although the variability in fat content in the ACVR2B/Fc-treated flight mice was too large for us to draw any conclusions regarding the effect of blocking this pathway on fat loss in microgravity. The effect of the decoy receptor on promoting muscle growth was also evident upon analysis of muscles at LAR, as weights of individual muscles were significantly higher in ACVR2B/Fc-treated flight mice even compared to uninjected ground mice (Fig. 1*B*). Although overall muscle weights in ACVR2B/Fc-treated flight mice were lower than in ACVR2B/Fc-treated ground mice, it is clear that blocking this signaling pathway is effective in increasing muscle growth in the setting of microgravity. Similar findings were recently reported in which a MSTN monoclonal antibody was shown to be capable of increasing muscle mass in mice in microgravity (25).

Unlike most other MSTN inhibitors, such as anti-MSTN monoclonal antibodies, the ACVR2B/Fc decoy receptor with its broader ligand specificity is capable of affecting not only skeletal muscle growth but also bone homeostasis. Indeed, treatment with ACVR2B/Fc resulted in substantial effects on bone mineral density in both ground and flight mice, which was apparent in comparing the data obtained from the two in-flight DXA scans on days L+6 and L+28 (Fig. 2*A*). Exposure of *wild type* mice to these 22 d of microgravity led to significant reductions in bone mineral density (BMD) of the whole body, left femur, and right femur by 8%, 11%, and 8%, respectively, compared to mice maintained on Earth. Bone mineral content (BMC) was also lower in flight mice compared to ground mice, and the reduction in BMC was apparent even by the time of the first in-flight DXA scans on day L+6 (Fig. 2*B*). Interestingly, BMD in the humerus was not reduced in flight mice during this 22 d period, consistent with the differential effects of microgravity on the femur and humerus reported in rats (26) and humans (27). Surprisingly, BMD in the humerus was even higher in flight mice compared to ground mice by the time of the first in-flight DXA scan on day L+6, with BMD of the left humerus being 14% higher in flight mice (Fig. 2*A*). Although additional studies will be required to understand the basis of this phenomenon, we speculate that this increase may reflect an adaptation in locomotion behavior in response to microgravity, with mice preferentially loading their forelimbs relative to their hindlimbs, as was also proposed by Maupin et al. (28), along with an overall increase in physical activity (such as circling and "race-tracking") observed for mice at the ISS (29). Consistent with this hypothesis, the relative magnitude of muscle loss was also greater in the lower body (quadriceps, gastrocnemius, soleus) compared to the upper body (triceps, pectoralis) (Fig. 1*B*). Treatment of ground mice with ACVR2B/Fc resulted in increases of whole body, left femur, and right femur BMD by 4%, 10%, and 9%, respectively (Fig. 2*A*). ACVR2B/Fc was also effective in increasing BMD in flight mice, with BMD being comparable in ACVR2B/Fc-treated flight mice compared to uninjected ground mice. Although BMD was generally lower in ACVR2B/Fc-treated flight mice than in ACVR2B/Fc-treated ground mice, the differential in BMD between ACVR2B/Fc-treated and uninjected mice was actually higher in flight mice than in ground mice, demonstrating that treatment with the decoy receptor afforded significant protection against bone loss due to microgravity.

This protective effect on bone was assessed in detail by microcomputed tomography (microCT) analysis of bones isolated at LAR. ACVR2B/Fc treatment increased bone mass of long bones and vertebrae not only in ground mice but also in flight mice (Fig. 2*C*). Quantitative analysis of the microCT images revealed that bone volume/total volume (BV/TV), trabecular thickness, trabecular number, and cortical thickness were all significantly reduced (by 37%, 8%, 9%, and 9%, respectively) in femurs of uninjected flight mice compared to uninjected ground mice (Table 1; see also *SI Appendix*, Table S1). These same parameters were increased significantly in ACVR2B/Fc-treated ground mice compared to uninjected ground mice (by 96%, 10%, 31%, and 12%, respectively). Strikingly, treatment of flight mice with ACVR2B/Fc not only led to dramatic increases in these parameters, but for two of these parameters (BV/TV

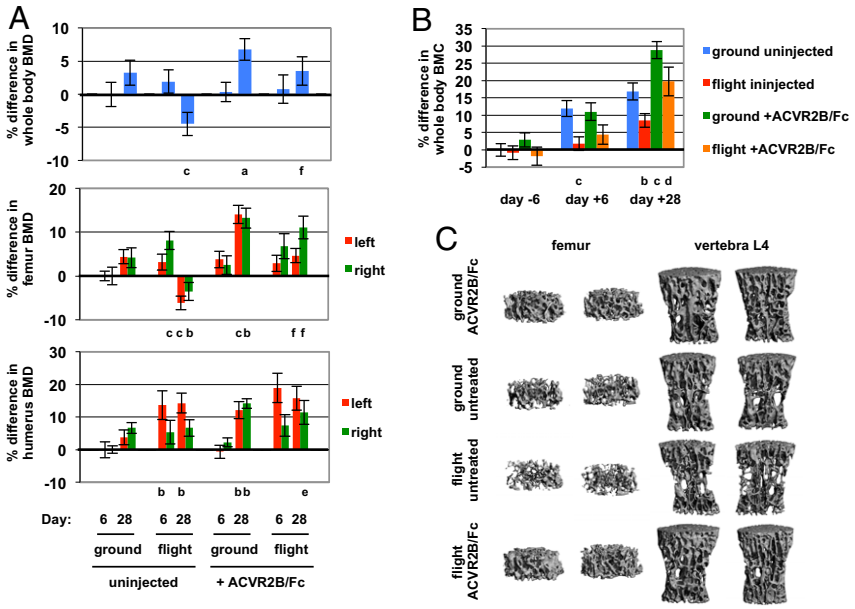

Fig. 2. Mitigation of bone loss in microgravity by targeting myostatin/activin A signaling. (*A*) Changes in bone mineral density between the two in-flight DXA scans on days L+6 and L+28. Percent differences were calculated relative to ground mice at day L+6 (i.e., all numbers were normalized to ground mice at day +6, which was set to zero). (*B*) Changes in BMC. Percent differences were calculated relative to ground mice at day L-6 (i.e., all numbers were normalized to ground mice at day L-6, which was set to zero). (*C*) Representative microCT images of femurs and L4 vertebrae. [a] $P < 0.05$, [b] $P < 0.01$, [c] $P < 0.001$ versus uninjected ground mice; [d] $P < 0.05$, [e] $P < 0.001$, [f] $P < 0.001$ versus ACVR2B/Fc-injected ground mice.

Table 1. MicroCT analysis

	Ground uninjected	Flight uninjected	Ground + ACVR2B/Fc	Flight + ACVR2B/Fc
Femur (trabecular)				
Bone volume fraction (BV/TV)	13.01 ± 0.75	8.26 ± 0.76[b]	25.56 ± 0.56[e]	25.84 ± 1.70[i]
Trabecular thickness (μm)	57.7 ± 1.1	53.0 ± 1.1[c]	63.5 ± 0.7[f]	60.1 ± 1.4[k,d]
Trabecular number (1/mm)	3.83 ± 0.09	3.47 ± 0.09[d]	5.02 ± 0.05[e]	5.27 ± 0.16[i]
Trabecular spacing (μm)	253.6 ± 6.1	286.7 ± 7.8[c]	191.3 ± 1.8[e]	180.3 ± 5.8[i]
Connectivity density (1/mm^3)	102.6 ± 5.7	81.8 ± 14.5	150.6 ± 6.0[e]	196.4 ± 8.1[m,b]
Apparent density (mg/ccm HA)	166.5 ± 8.1	108.6 ± 6.5[a]	282.7 ± 4.9[e]	275.8 ± 16.6[i]
Tissue density (mm^3)	931.3 ± 6.3	899.4 ± 6.8[c]	929.4 ± 5.6	910.6 ± 6.3[d]
Total volume (mm^3)	2.03 ± 0.03	2.19 ± 0.04[c]	2.06 ± 0.03	2.24 ± 0.02[b]
Bone volume (mm^3)	0.264 ± 0.015	0.182 ± 0.019[c]	0.526 ± 0.017[e]	0.579 ± 0.039[i]
Structure model index	2.19 ± 0.09	2.80 ± 0.17[c]	0.79 ± 0.10[e]	0.72 ± 0.16[i]
Bone surface (mm^2)	12.57 ± 0.55	9.80 ± 0.87[d]	20.09 ± 0.59[e]	23.34 ± 0.82[m,c]
Specific bone surface (mm^2)	48.85 ± 1.07	56.35 ± 1.20[b]	38.35 ± 0.49[e]	40.84 ± 1.33[i]
Bone surface density (1/mm)	6.21 ± 0.25	4.45 ± 0.33[b]	9.76 ± 0.16[e]	10.42 ± 0.35[i]
BS/MV (1/mm)	7.15 ± 0.36	4.87 ± 0.41[b]	13.13 ± 0.30[e]	14.17 ± 0.83[i]
Degree of anisotropy	1.42 ± 0.02	1.32 ± 0.02[b]	1.54 ± 0.03[g]	1.56 ± 0.02[i]
L4 vertebrae				
Bone volume fraction (BV/TV)	29.00 ± 0.67	20.82 ± 0.77[a]	36.52 ± 0.63[e]	35.09 ± 1.01[i]
Trabecular thickness (μm)	54.0 ± 1.1	46.6 ± 0.6[a]	59.5 ± 0.9[g]	57.9 ± 1.3[i]
Trabecular number (1/mm)	4.94 ± 0.07	4.62 ± 0.08[c]	5.79 ± 0.04[e]	5.66 ± 0.10[i]
Trabecular spacing (μm)	190.3 ± 3.6	208.3 ± 4.4[c]	163.5 ± 1.6[e]	167.7 ± 3.3[i]
Connectivity density (1/mm^3)	214.1 ± 9.3	230.1 ± 9.3	258.8 ± 10.9[g]	251.9 ± 16.6
Apparent density (mg/ccm HA)	328.3 ± 8.2	242.1 ± 7.5[a]	396.8 ± 6.6[e]	384.7 ± 9.4[i]
Tissue density (mm^3)	948.8 ± 5.3	925.0 ± 2.4[c]	941.4 ± 4.6	939.2 ± 3.8[k]
Total volume (mm^3)	2.29 ± 0.04	2.26 ± 0.06	2.28 ± 0.06	2.30 ± 0.07
Bone volume (mm^3)	0.664 ± 0.025	0.471 ± 0.024[a]	0.832 ± 0.027[f]	0.809 ± 0.041[i]
Structure model index	−0.06 ± 0.05	0.77 ± 0.07[a]	−0.75 ± 0.10[e]	−0.54 ± 0.11[i]
Bone surface (mm^2)	27.21 ± 0.66	23.73 ± 1.02[c]	30.25 ± 0.88[h]	30.31 ± 1.16[j]
Specific bone surface (mm^2)	40.98 ± 0.85	50.80 ± 0.81[a]	36.22 ± 0.72[f]	37.47 ± 1.04[i]
Bone surface density (1/mm)	11.89 ± 0.12	10.49 ± 0.29[b]	13.27 ± 0.09[e]	13.15 ± 0.19[i]
BS/MV (1/mm)	16.76 ± 0.28	13.28 ± 0.48[a]	20.92 ± 0.24[e]	20.30 ± 0.50[i]
Degree of anisotropy	1.87 ± 0.03	1.92 ± 0.02	1.76 ± 0.03[h]	1.75 ± 0.04[k]

[a] $P < 10^{-4}$, [b] $P < 10^{-3}$, [c] $P < 0.01$, [d] $P < 0.05$ vs. corresponding ground cohort. [e] $P < 10^{-4}$, [f] $P < 10^{-3}$, [g] $P < 0.01$, [h] $P < 0.05$ vs. ground uninjected. [i] $P < 10^{-4}$, [j] $P < 10^{-3}$, [k] $P < 0.01$, [m] $P < 0.05$ vs. flight uninjected.

and trabecular number), the absolute numbers were nearly indistinguishable from those of ACVR2B/Fc-treated ground mice; that is, for BV/TV and trabecular number for the femurs, there appeared to be minimal effect of microgravity, implying ACVR2B/Fc treatment rendered the femurs completely resistant to the effect of microgravity. Similar effects were also seen in humeri, although trabecular thickness in humeri was unaffected by ACVR2B/Fc treatment in either ground or flight mice (*SI Appendix*, Table S2). The protective effect of ACVR2B/Fc was seen in L4 vertebrae as well (Table 1). Although there was a trend toward lower numbers in ACVR2B/Fc-treated flight mice compared to ACVR2B/Fc-treated ground mice, none of the differences were statistically significant, suggesting that the vertebrae seemed to be largely protected from microgravity-induced loss, which was most evident when considering the differential between untreated and ACVR2B/Fc-treated values in the flight groups. Similar results were obtained on analysis of L2, L3, and L5 vertebrae (*SI Appendix*, Tables S3–S5). Hence, blockade of MSTN/activin A signaling by treatment with the ACVR2B/Fc decoy receptor can dramatically increase bone mass even in the setting of microgravity and, furthermore, can protect against bone loss caused by microgravity.

The bone protective effects of the ACVR2B/Fc decoy receptor could be a direct effect of inhibition of ligands signaling to bone and/or an indirect effect of enhanced muscling resulting in increased mechanical load on the bones. To assess the contribution of the latter, we analyzed the effect of microgravity on the bones of *Mstn* $^{-/-}$ mice. Despite the dramatic muscling seen in these mice, BV/TV, trabecular thickness, and apparent density were actually lower in both the femurs and vertebrae of *Mstn* $^{-/-}$ mice (see *SI Appendix*, Table S6), most likely as a result of the unusual musculature in these mice. In *Mstn* $^{-/-}$ mice exposed to microgravity, BV/TV and trabecular number were lower in both the femurs and vertebrae compared to *Mstn* $^{-/-}$ ground mice, although the magnitude of the differences was smaller than that seen in *wild type* flight mice compared to *wild type* ground mice. Moreover, trabecular thickness in *Mstn* $^{-/-}$ mice was similar between the flight and ground groups. Hence, although the increased muscling in *Mstn* $^{-/-}$ mice may have afforded partial protection from bone loss due to microgravity, our findings imply that the near complete protection seen in mice treated with ACVR2B/Fc likely reflects inhibition of signaling by ligands other than MSTN directly to bone.

In addition to examining the effect of blocking this pathway on muscle and bone loss during spaceflight, we also examined the effect of administering ACVR2B/Fc to mice after return to Earth. Lean body mass (Fig. 3*A*) and muscle weights (Fig. 3*B*) of mice were completely restored to baseline levels following 2 wk on Earth even in the absence of treatment, suggesting that mice recover lost muscle mass quickly after return to gravity; however, because we did not measure body water content, we cannot rule out the possibility that shifts in water content may account for this apparent rapid recovery. Treatment of mice with ACVR2B/Fc greatly potentiated the recovery of muscle mass, with weights of pectoralis, triceps, quadriceps, gastrocnemius/plantaris, and soleus muscles going from 8%, 8%, 15%, 14%, and 18%, respectively, below baseline at LAR to 39%, 36%, 34%, 26%, and 20%, respectively, above baseline 2 wk after treatment on Earth.

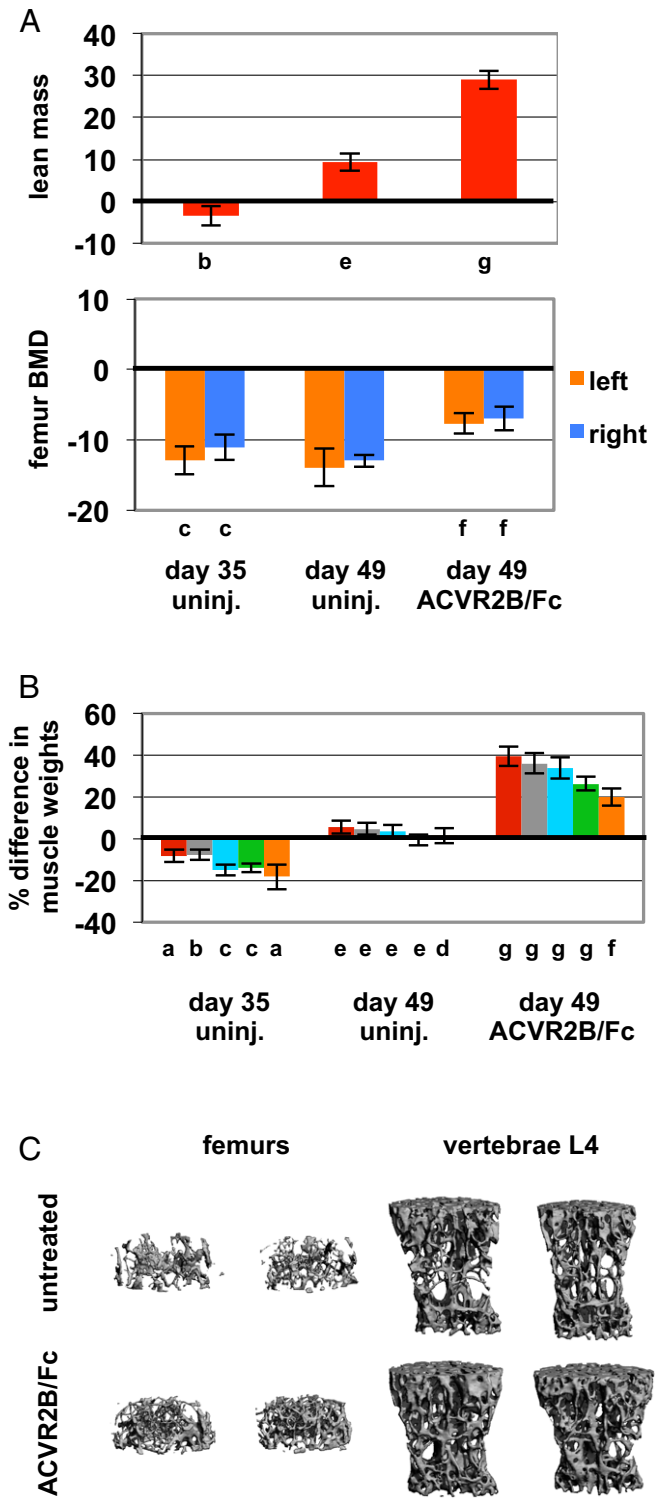

Fig. 3. Recovery of muscle and bone mass during the 2-wk recovery period following return to Earth. Effect of 14 d of treatment with ACVR2B/Fc on (*A*) lean body mass and femur BMD (by DXA), (*B*) muscle weights, and (*C*) femurs and L4 vertebrae (by microCT). Bars in *B* represent pectoralis (red), triceps (gray), quadriceps (blue), gastrocnemius/plantaris (green), and soleus (orange) muscles. Numbers represent percent differences relative to uninjected ground mice at LAR (i.e., all numbers were normalized to uninjected ground mice at day L+35, which was set to zero). [a] $P < 0.05$, [b] $P < 0.01$, [c] $P < 0.001$ versus uninjected ground mice at LAR; [d] $P < 0.01$, [e] $P < 0.001$ versus uninjected flight mice at LAR; [f] $P < 0.01$, [g] $P < 0.001$ versus uninjected flight mice on day 49.

In the case of bone, not only did mice fail to recover lost bone mass during the 2 wk recovery period, but they even appeared to continue to lose additional bone mass after return to Earth (*SI Appendix*, Table S6). Treatment with ACVR2B/Fc, however, led to significant conservation or gain of bone mass during this recovery period, with many of the parameters being partially or entirely restored after 2 wk of treatment, which was apparent even on gross examination of the microCT images of the femurs and vertebrae (Fig. 3*C*). Hence, ACVR2B/Fc was effective in promoting recovery of both muscle and bone mass following spaceflight. This effect of ACVR2B/Fc on recovery of bone mass is significant given that restoring bone health can pose a challenge for astronauts returning from space missions (30).

The effects of blocking MSTN/activin signaling in microgravity were also reflected at the molecular level. We carried out proteomic analysis of plasma using the SomaScan assay, which uses aptamers to measure relative levels of over 5,000 secreted proteins (31). A comparison of plasma samples between ACVR2B/Fc-treated and uninjected mice on Earth revealed a large number of differences, which depended not only on the *P* value cutoff used to assign statistical significance but also on the duration of treatment. A list of the 50 most down-regulated and 50 most up-regulated proteins in ground mice treated with ACVR2B/Fc for 5 wk is shown in *SI Appendix*, Tables S7 and S8. Visualizing these differences by the corresponding heat map (Fig. 4*A*) showed that many of these differences were also seen in mice treated with ACVR2B/Fc for 1 wk or 2 wk. Moreover, when the differences were sorted based on the top up-regulated and down-regulated proteins at the 1 wk time point, the overall pattern generally persisted in subsequent time points. Finally, the patterns seen in ACVR2B/Fc-treated ground mice were also very similar to the patterns seen in flight mice injected with ACVR2B/Fc. These similarities were evident in comparisons of ratios for all proteins as well as in heat maps corresponding to just the most up-regulated and down-regulated proteins and were seen in mice that were injected either during flight or during the recovery period following return to Earth (Fig. 4*A*). These results are consistent with ACVR2B/Fc having similar effects in microgravity as on Earth.

Among the down-regulated proteins in ground mice at 1, 2, and 5 wk of treatment were MSTN, activin AB, and BMP-9 (Fig. 4*B* and *SI Appendix*, Table S7), which likely reflected clearance of these proteins by binding to ACVR2B/Fc. This was almost certainly the case for MSTN, as *Mstn* RNA levels were actually increased in muscles of ACVR2B/Fc-treated mice (Fig. 4*C*), and skeletal muscle is by far the main source of circulating MSTN protein. In this regard, the expression of *Gdf11*, which is highly related to *Mstn*, was also up-regulated not only in muscle but also in bone. Other TGF-β family members were down-regulated in the plasma of ACVR2B/Fc-treated mice, including BMP-4, BMP-6, BMP-7, and TGFβ1 (Fig. 4*B* and *SI Appendix*, Table S7), none of which are known to be capable of binding ACVR2B (32).

In addition to the TGF-β family, components of several other key pathways were also modulated in ACVR2B/Fc-treated mice. Strikingly, the first and fourth most up-regulated proteins in the plasma of ACVR2B/Fc-treated ground mice were two known ligands of osteoprotegerin (OPG), namely TRAIL (tumor necrosis factor ligand superfamily member 10) and RANKL (tumor necrosis factor ligand superfamily member 11), which were increased by 474% and 172%, respectively (Fig. 5*A* and *SI Appendix*, Table S8). Although we do not know the tissue source of these proteins in the plasma, RNA expression for TRAIL was up-regulated in both muscle and bone, and RNA for RANKL was up-regulated in bone [RANKL was not detected by RNA sequencing (RNAseq) analysis in muscle] (Fig. 5*B*). Because TRAIL and RANKL are known to regulate osteoclast differentiation and survival (33–35), these findings suggest that increased RANK (tumor necrosis factor receptor superfamily member 11a) signaling may be involved in the regulation of bone

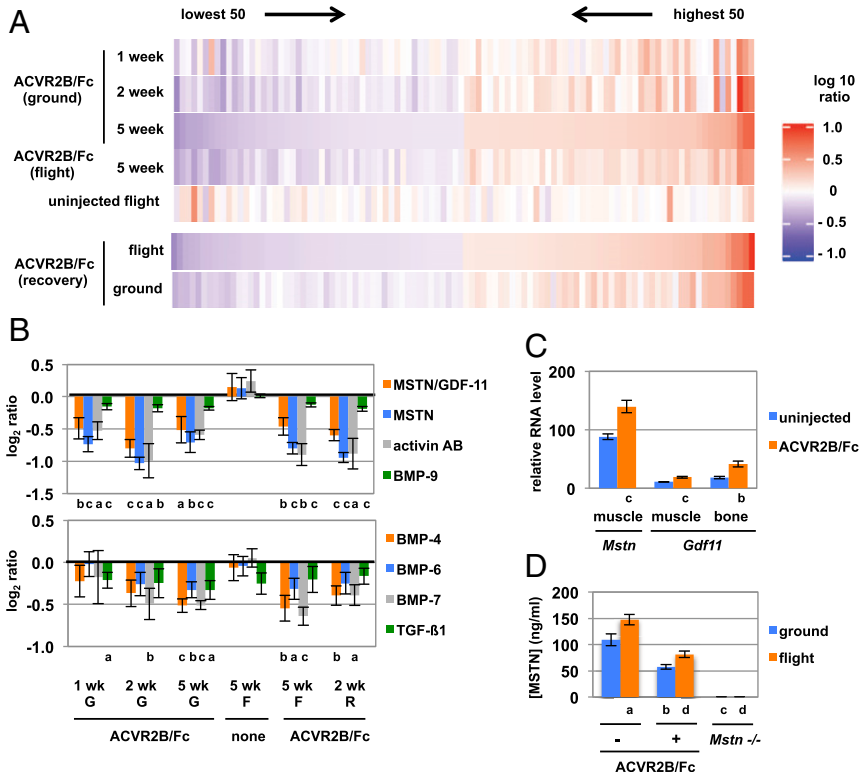

Fig. 4. Changes in plasma protein profiles as a result of ACVR2B/Fc treatment and microgravity. (*A*) Heat maps showing the 50 most up-regulated and 50 most down-regulated proteins identified by SomaScan analysis and sorted by ACVR2B/Fc-treated versus uninjected ground mice at 5 wk (*Upper* group of 5 heat maps) or by ACVR2B/Fc-treated versus uninjected flight mice during the 2-wk recovery period after return to Earth (*Lower* group of two heat maps). (*B*) Differences in plasma levels of TGF-β family members. Numbers indicate $\log_2$ of the ratios of protein levels determined by SomaScan analysis in ACVR2B/Fc-treated versus uninjected mice or flight versus ground uninjected mice. (*C*) Relative RNA levels of *Mstn* and *Gdf11* in muscle and/or bone determined by RNAseq analysis. (*D*) Plasma concentrations of MSTN determined by ELISA. G, ground; F, flight; R, recovery. [a] $P < 0.05$, [b] $P < 0.01$, [c] $P < 0.001$ versus uninjected ground mice; [d] $P < 0.001$ versus uninjected flight mice.

growth and remodeling induced by ACVR2B/Fc. Interestingly, the third known ligand for OPG, von Willebrand factor (VWF), was the eighth most up-regulated protein (increased by 132%; *SI Appendix*, Table S8). Although mice lacking VWF have been reported to have normal bone density (36), transgenic mice expressing a mutant form of the protein corresponding to that seen in patients with platelet-type von Willebrand disease exhibit a high bone mass phenotype (37). It is also known that mice (and patients) with hemophilia due to lack of clotting factor VIII or IX are osteoporotic and osteopenic (36, 38).

Because OPG itself was not identified in the proteomic analysis, with the signals being below the limit of detection in the assay, we used an enzyme-linked immunosorbent assay (ELISA) to measure OPG levels. Although there were no statistically significant differences between ACVR2B/Fc-treated and uninjected ground mice or between uninjected flight and ground mice, OPG levels were increased by 24% in ACVR2B/Fc-treated compared to uninjected flight mice (Fig. 5*C*). The greatest differences were observed in comparisons of *Mstn* $^{-/-}$ versus uninjected mice, with OPG levels being increased by 72% and 40% in *Mstn* $^{-/-}$ flight and ground mice, respectively. In addition to the role that OPG plays in modulating RANK signaling in osteoclasts, OPG has been shown to be capable of increasing muscle force when given to *mdx* mice (39, 40), which is a model for muscular dystrophy, raising the possibility that OPG may play a role in muscle hypertrophy induced by loss of MSTN/activin A signaling. In this regard, the effect of OPG on *mdx* muscle was reported to be greater than that induced by coadministration of anti-RANKL and anti-TRAIL antibodies and was also seen in mice in which RANK had been targeted in muscle, suggesting that OPG acts at least partly in a RANK-independent manner to regulate muscle function (40).

Among the most down-regulated proteins in ACVR2B/Fc-treated mice were components of other signaling pathways also known to be important for maintaining bone homeostasis. In particular, two hedgehog isoforms, IHH and SHH, were down-regulated in ground mice following ACVR2B/Fc treatment for 1, 2, and 5 wk as well as in mice treated either during flight or during the recovery period following return to Earth (Fig. 5*A* and *SI Appendix*, Table S7). In addition to the roles that IHH and SHH play in regulating bone development, hedgehog signaling is also important for maintaining bone homeostasis in adult mice, with down-regulation of hedgehog signaling being protective against bone loss (41, 42). Also striking in the plasma analysis was that aptamers directed against three Dickkopf isoforms, DKK1, DKK2, and DKK4, corresponded to the second, third, and 10th most down-regulated signals, respectively, in ACVR2B/Fc-treated mice (Fig. 5*A* and *SI Appendix*, Table S7). Because the aptamers for DKK2 and DKK4 show some cross-reactivity to human DKK1, additional studies will be required to determine whether the three aptamers were all detecting differences in levels of DKK1. Nevertheless, given that Dickkopfs are secreted proteins capable of antagonizing Wnt signaling by inhibiting the coreceptors LRP5 and LRP6 (43, 44), these findings suggest that increased Wnt signaling may also be involved in the increase in bone mass induced by ACVR2B/Fc. Consistent with this possibility, two other Wnt inhibitors, namely sFRP1 and

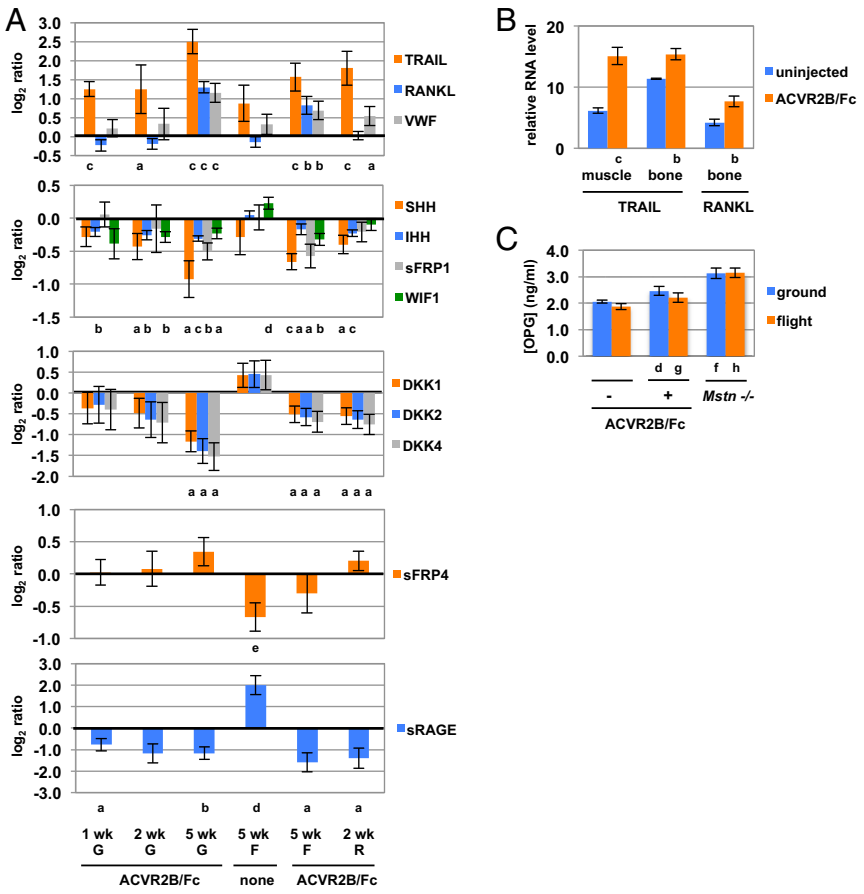

Fig. 5. Changes in protein and RNA levels for components of RANK, hedgehog, Wnt, and RAGE signaling pathways. (*A*) Log_2 of the ratios of protein levels determined by SomaScan analysis in ACVR2B/Fc-treated versus uninjected mice or flight versus ground uninjected mice. (*B*) Relative RNA levels of TRAIL and RANKL in muscle and/or bone determined by RNAseq analysis. (*C*) Plasma concentrations of OPG determined by ELISA. G, ground; F, flight; R, recovery. [a] $P < 0.05$, [b] $P < 0.01$, [c] $P < 0.001$ versus uninjected mice; [d] $P < 0.05$, [e] $P < 0.01$, [f] $P < 0.001$ versus uninjected ground mice; [g] $P < 0.05$, [h] $P < 0.001$ versus uninjected flight mice.

WIF1, were also down-regulated as a result of ACVR2B/Fc treatment (Fig. 5*A*).

Levels of Wnt signaling components were also modulated as a result of exposure to microgravity. For example, in contrast to what was seen in ACVR2B/Fc-treated mice, WIF1 was up-regulated in flight compared to ground uninjected mice (Fig. 5*A*). Moreover, the most down-regulated protein in response to microgravity was sFRP4 (secreted Frizzled-related protein 4), which was decreased by 37% in flight mice compared to ground mice (Fig. 5*A* and *SI Appendix*, Table S9). sFRP4 is known to be a Wnt regulator, and mutations in *SFRP4* in humans have been shown to cause Pyle disease, which is characterized by cortical bone fragility and fractures (45). Mice lacking sFRP4 exhibit increased trabecular bone mass but reduced cortical bone thickness and failure of bone remodeling (46). Given that loss-of-function mutations in the Wnt receptor LRP5 results in low bone mass in both humans (47) and mice (48), the down-regulation of sFRP4, taken together with changes in levels of several Wnt inhibitors, suggests that altered Wnt signaling may play a role in bone loss resulting from exposure to microgravity and that the protective effect of ACVR2B/Fc on microgravity-induced bone loss may result at least in part by shifting the balance of Wnt regulators. Increasing Wnt signaling has also been shown to be capable of driving muscle hypertrophy (49), raising the possibility that modulation of levels of these Wnt regulators systemically may also have contributed to muscle growth induced by ACVR2B/Fc.

In addition to the Wnt pathway, another signaling pathway implicated in the comparison of plasma profiles between flight and ground mice was that mediated by RAGE, which is a transmembrane receptor for advanced glycosylation end products (50). sRAGE, which is a naturally occurring truncated form of the receptor, was the top up-regulated protein in response to microgravity (*SI Appendix*, Table S10), being increased by 251% in flight compared to ground mice (Fig. 5*A*). The elevation in sRAGE, which plays a role in inflammation, may reflect the extensive stress to which these mice were subjected, not only in terms of time spent in microgravity but also in terms of the rapid changes in g forces experienced by the mice during lift-off and return. In this respect, another top up-regulated protein in flight mice was POMC (*SI Appendix*, Table S10), which ultimately is involved in mediating the cortisol stress response. In addition to having a proinflammatory role, however, RAGE signaling is also known to be important in regulating bone resorption, and mice lacking RAGE have been shown to have increased bone mass and bone mineral density (51). Although increased levels of sRAGE might be expected to inhibit bone resorption, circulating levels of sRAGE have been shown to correlate with osteopenia, osteoporosis, and bone fragility, which has led to the suggestion that increased sRAGE levels in the blood may reflect increased osteoclast activity systemically (52). Interestingly, sRAGE was also the first and fourth most down-regulated protein (decreased by 67% and 56%) in ACVR2B/Fc-treated flight and ground mice, respectively (Fig. 5*A* and *SI Appendix*, Table S7). The fact that sRAGE levels are counter regulated in microgravity versus ACVR2B/Fc treatment suggests that plasma sRAGE levels may

be an indicator of the opposite effects occurring in bone in these two conditions.

Finally, as discussed earlier, the SomaScan assay detected MSTN itself as one of the down-regulated proteins in the plasma of ACVR2B/Fc-treated mice. Because the effect of microgravity on MSTN levels was inconclusive in this assay, we measured MSTN concentrations by ELISA. Consistent with the SomaScan results, the ELISA showed that MSTN levels were decreased by about 50% in ACVR2B/Fc-treated compared to uninjected ground and flight mice (Fig. 4*D*). Most significantly, the ELISA showed that plasma MSTN levels were higher in uninjected flight mice compared to uninjected ground mice by 35%. This finding raises the intriguing possibility that MSTN itself may be one of the mediators of muscle loss induced by microgravity. In this respect, the 28th most up-regulated protein by SomaScan analysis in flight mice was BMP-1 (*SI Appendix*, Table S10), which would be predicted to increase activation of latent MSTN by proteolytic cleavage of the MSTN propeptide (53).

In addition to the proteomic analysis of plasma, we carried out RNAseq analysis of both bone and skeletal muscle, which revealed numerous changes in RNA expression patterns as a result of ACVR2B/Fc treatment and exposure to microgravity. A summary of the top 50 down-regulated and top 50 up-regulated genes in muscle and bone is shown in *SI Appendix*, Tables S7–S10. A pathway analysis of differentially expressed genes in bone as a result of ACVR2B/Fc treatment in ground mice is shown in Fig. 6. Among the pathways that were identified in this analysis were four of the signaling pathways implicated by the SomaScan findings in plasma, namely Wnt, TGF-β, RAGE, and hedgehog signaling pathways, consistent with the dramatic effects of the decoy receptor on bone homeostasis. Pathway analysis of differentially regulated genes in muscle as a result of ACVR2B/Fc treatment revealed a number of key pathways known to be involved in regulating muscle homeostasis, such as the FoxO, P13K-Akt, MAPK, and insulin signaling pathways (*SI Appendix*, Fig. S1). None of the signaling pathways identified in the SomaScan findings, however, were identified by this pathway analysis of RNAseq data for muscle. Consistent with this difference between bone and muscle, for example, was that key hedgehog signaling components were up-regulated in bone but not in muscle (Fig. 7*A*).

Pathway analysis of differentially regulated genes as a result of exposure to microgravity also revealed a number of key pathways in both bone and muscle (*SI Appendix*, Figs. S2 and S3). Although pathway analysis of neither bone nor muscle identified any of the pathways implicated by the SomaScan findings in plasma, numerous key signaling components for some of these pathways were clearly differentially regulated in both bone and muscle. In the case of the TGF-β signaling pathway, many regulatory components were up-regulated in both bones and muscles of flight mice, including many of the receptors for this group of ligands (Fig. 7*B*). Similarly, numerous Wnt regulatory components were also either up- or down-regulated in flight mice in both bone and muscle (Fig. 7*C*).

Taken together, these studies suggest that exposure to microgravity leads to alterations in multiple signaling pathways affecting skeletal muscle and bone homeostasis and that alterations in many of the key pathways are evident even in the profile of proteins in the plasma. Targeting the MSTN/activin A signaling pathway can also have major effects in changing expression patterns corresponding to these signaling pathways, including in the plasma, and can have a significant effect in protecting against muscle and bone loss during spaceflight as well as promoting recovery of muscle and bone mass following spaceflight. We believe that these findings have implications for utilizing this therapeutic strategy to combat simultaneously both muscle and bone loss, not only in people suffering from disuse atrophy on Earth, such as in bedridden, wheelchair-bound, and older individuals, but also in astronauts on long duration space missions.

Materials and Methods

All animal experiments were carried out in accordance with protocols that were approved by the Institutional Animal Care and Use Committees at NASA, The Jackson Laboratory, the University of Connecticut, and Explora Biolabs. *Wild type* C57BL/6N and *Mstn* $^{-/-}$ mice (backcrossed onto a C57BL/6N genetic background) were bred at The Jackson Laboratory and sent to Kennedy Space Center ~5 wk prior to launch. All mice were 70 ($^{+/-}$2) days old on the day of launch (L+0). Mice were assigned to five groups of eight animals as follows: uninjected C57BL/6N mice (groups 1, 4, and 5), ACVR2B/Fc-treated C57BL/6N mice (group 3), and *Mstn* $^{-/-}$ mice (group 2). Mice in groups 1, 2, and 3 were all euthanized for analysis at LAR, and mice in groups 4 and 5 were maintained live at Explora for an additional 14 d after LAR. Identical ground control mice corresponding to groups 1 to 3 were maintained at KSC under the same

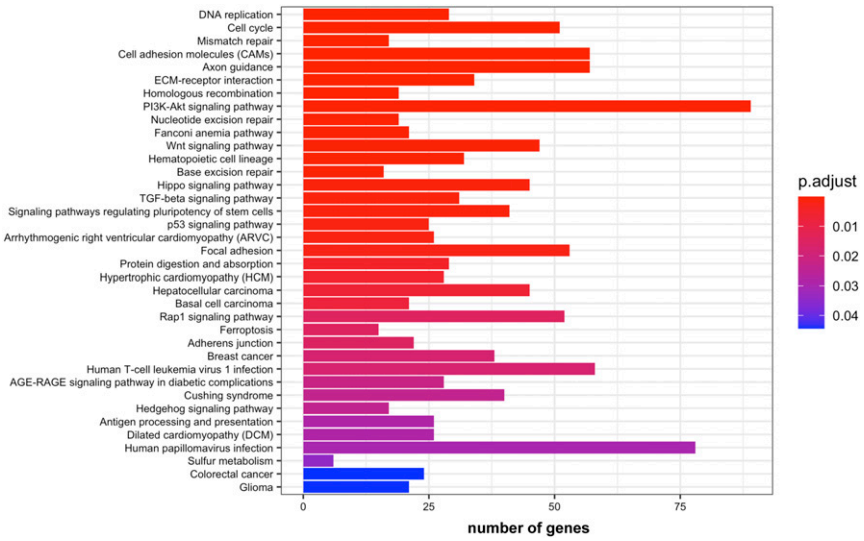

Fig. 6. RNAseq analysis. Bar graph showing the top 37 pathways in bone exhibiting differentially expressed transcripts between ACRVR2B/Fc-treated and uninjected ground mice. Pathways are rank-ordered based on *P* values. Sizes of bars indicate the number of genes within a pathway showing statistically significant differences.

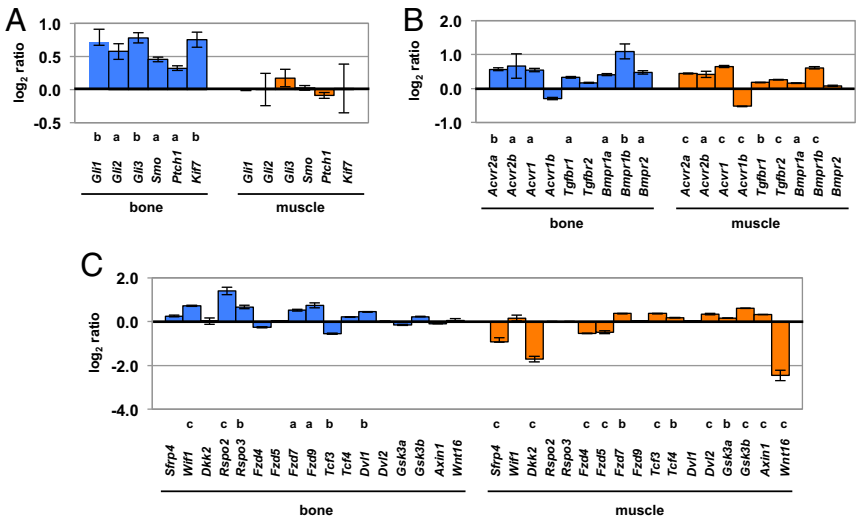

Fig. 7. Relative RNA levels of various components of the (*A*) hedgehog, (*B*) TGF-β family, and (*C*) Wnt signaling pathways. Numbers indicate $\log_2$ of the ratios of RNA levels determined by RNAseq analysis of ACVR2B/Fc-treated versus uninjected mice (in *A*) or flight versus ground uninjected mice (in *B* and *C*). [a] $P < 0.05$, [b] $P < 0.01$, [c] $P < 0.001$ versus uninjected (in *A*) or ground (in *B* and *C*) mice.

environmental conditions as those recorded for flight mice aboard the ISS. The ACVR2B/Fc decoy receptor was expressed in Chinese hamster ovary cells, purified from the conditioned medium using a protein A Sepharose column, and administered intraperitoneally at a dose of 175 μg per injection. Mice in group 3 were injected with ACVR2B/Fc on days L-3, L+5, L+11, L+17, L+22, and L+28/29. Mice in group 5 were injected with ACVR2B/Fc on days L+35 and L+42. In order to limit astronaut time aboard the ISS, we used uninjected rather than vehicle-injected mice as controls. Live animal imaging was performed using a Piximus DXA on all 40 mice on days L-6 and L+35. Two in-flight DXA scans were performed on mice in groups 1 and 3 on days L+6/7 and L+28/29. Final post-recovery DXA scans were performed on mice in groups 4 and 5 on day L+49. Muscle weight, microCT, RNAseq, SomaScan, and ELISA analyses are described in detail in *SI Appendix*.

Data Availability. The RNAseq and proteomic data were deposited in the NCBI Sequence Read Archive (SRA BioProject ID PRJNA656237) and Gene Expression Omnibus (GEO accession number GSE156321), respectively.

ACKNOWLEDGMENTS. We thank Michael Roberts, Jennifer Finkel, William McLamb, Terri Bauer, Cole Nelson, Nicolas Cole, Raquel Jaeger, Melissa Rhodes, Alonso Fuentes, Hailey Willey, Jessica Gray, William Therrien, Kellie Leonard, Joe Bielitzki, Russell Higbee, Ramona Bober, Autumn Cdebaca, Mary Lou James, Grishma Acharya, Alixandra Borgert, Susie Airhart, and Sheila Bourgeois for all their help throughout this mission. Research reported in this publication was supported by the International Space Station U.S. National Laboratory under agreement number UA-2019-031, by a Director's Innovation Fund grant from The Jackson Laboratory (to S.-J.L.), by NIH grants R01AR060636 and R01AG052962 (to S.-J.L.), and by funds from UConn Health (E.L.G.-L. and S.-J.L.) and Connecticut Children's (E.L.G.-L.).

1. S.-J. Lee, "Myostatin: Regulation, function, and therapeutic applications" in *Muscle: Fundamental Biology and Mechanisms of Disease*, J. A. Hill, E. N. Olson, Eds. (Academic Press, 2012), pp. 1077–1084.
2. A. C. McPherron, A. M. Lawler, S.-J. Lee, Regulation of skeletal muscle mass in mice by a new TGF-β superfamily member. *Nature* **387**, 83–90 (1997).
3. A. C. McPherron, S.-J. Lee, Double muscling in cattle due to mutations in the myostatin gene. *Proc. Natl. Acad. Sci. U.S.A.* **94**, 12457–12461 (1997).
4. L. Grobet *et al.*, A deletion in the bovine myostatin gene causes the double-muscled phenotype in cattle. *Nat. Genet.* **17**, 71–74 (1997).
5. R. Kambadur, M. Sharma, T. P. L. Smith, J. J. Bass, Mutations in myostatin (GDF8) in double-muscled Belgian Blue and Piedmontese cattle. *Genome Res.* **7**, 910–916 (1997).
6. A. Clop *et al.*, A mutation creating a potential illegitimate microRNA target site in the myostatin gene affects muscularity in sheep. *Nat. Genet.* **38**, 813–818 (2006).
7. D. S. Mosher *et al.*, A mutation in the myostatin gene increases muscle mass and enhances racing performance in heterozygote dogs. *PLoS Genet.* **3**, e79 (2007).
8. Q. Lv *et al.*, Efficient generation of myostatin gene mutated rabbit by CRISPR/Cas9. *Sci. Rep.* **6**, 25029 (2016).
9. H. Gu *et al.*, Establishment and phenotypic analysis of an Mstn knockout rat. *Biochem. Biophys. Res. Commun.* **477**, 115–122 (2016).
10. K. Wang *et al.*, CRISPR/Cas9-mediated knockout of myostatin in Chinese indigenous Erhualian pigs. *Transgenic Res.* **26**, 799–805 (2017).
11. Z. He *et al.*, Use of CRISPR/Cas9 technology efficiently targetted goat myostatin through zygotes microinjection resulting in double-muscled phenotype in goats. *Biosci. Rep.* **38**, BSR20180742 (2018).
12. M. Schuelke *et al.*, Myostatin mutation associated with gross muscle hypertrophy in a child. *N. Engl. J. Med.* **350**, 2682–2688 (2004).
13. S.-J. Lee *et al.*, Regulation of muscle growth by multiple ligands signaling through activin type II receptors. *Proc. Natl. Acad. Sci. U.S.A.* **102**, 18117–18122 (2005).
14. S.-J. Lee, Quadrupling muscle mass in mice by targeting TGF-β signaling pathways. *PLoS One* **2**, e789 (2007).
15. S.-J. Lee *et al.*, Regulation of muscle mass by follistatin and activins. *Mol. Endocrinol.* **24**, 1998–2008 (2010).
16. E. Latres *et al.*, Activin A more prominently regulates muscle mass in primates than does GDF8. *Nat. Commun.* **8**, 15153 (2017).
17. S.-J. Lee, A. C. McPherron, Regulation of myostatin activity and muscle growth. *Proc. Natl. Acad. Sci. U.S.A.* **98**, 9306–9311 (2001).
18. A. Koncarevic *et al.*, A soluble activin receptor type IIb prevents the effects of androgen deprivation on body composition and bone health. *Endocrinology* **151**, 4289–4300 (2010).
19. C. S. Chiu *et al.*, Increased muscle force production and bone mineral density in ActRIIB-Fc-treated mature rodents. *J. Gerontol. A Biol. Sci. Med. Sci.* **68**, 1181–1192 (2013).
20. B. C. Goh *et al.*, Activin receptor type 2A (ACVR2A) functions directly in osteoblasts as a negative regulator of bone mass. *J. Biol. Chem.* **292**, 13809–13822 (2017).
21. D. J. DiGirolamo, V. Singhal, X. Chang, S. J. Lee, E. L. Germain-Lee, Administration of soluble activin receptor 2B increases bone and muscle mass in a mouse model of osteogenesis imperfecta. *Bone Res.* **3**, 14042 (2015).
22. Y. Jeong *et al.*, Skeletal response to soluble activin receptor type IIB in mouse models of osteogenesis imperfecta. *J. Bone Miner. Res.* **33**, 1760–1772 (2018).
23. S. M. Smith *et al.*, Benefits for bone from resistance exercise and nutrition in long-duration spaceflight: Evidence from biochemistry and densitometry. *J. Bone Miner. Res.* **27**, 1896–1906 (2012).
24. J. Sibonga *et al.*, Resistive exercise in astronauts on prolonged spaceflights provides partial protection against spaceflight-induced bone loss. *Bone* **128**, 112037 (2019).
25. R. C. Smith *et al.*, Inhibition of myostatin prevents microgravity-induced loss of skeletal muscle mass and strength. *PLoS One* **15**, e0230818 (2020).
26. J. A. Keune, A. J. Branscum, U. T. Iwaniec, R. T. Turner, Effects of spaceflight on bone microarchitecture in the axial and appendicular skeleton in growing ovariectomized rats. *Sci. Rep.* **5**, 18671 (2015).
27. M. Stavnichuk, N. Mikolajewicz, T. Corlett, M. Morris, S. V. Komarova, A systematic review and meta-analysis of bone loss in space travelers. *NPJ Microgravity* **6**, 13 (2020).
28. K. A. Maupin *et al.*, Skeletal adaptations in young male mice after 4 weeks aboard the International Space Station. *NPJ Microgravity* **5**, 21 (2019).
29. A. E. Ronca *et al.*, Behavior of mice aboard the international space station. *Sci. Rep.* **9**, 4717 (2019).
30. E. S. Orwoll *et al.*, Skeletal health in long-duration astronauts: Nature, assessment, and management recommendations from the NASA bone summit. *J. Bone Miner. Res.* **28**, 1243–1255 (2013).
31. L. Gold *et al.*, Aptamer-based multiplexed proteomic technology for biomarker discovery. *PLoS One* **5**, e15004 (2010).

32. D. Sako *et al*., Characterization of the ligand binding functionality of the extracellular domain of activin receptor type IIb. *J. Biol. Chem.* **285**, 21037–21048 (2010).
33. W. J. Boyle, W. S. Simonet, D. L. Lacey, Osteoclast differentiation and activation. *Nature* **423**, 337–342 (2003).
34. G. Zauli *et al*., TRAIL inhibits osteoclastic differentiation by counteracting RANKL-dependent p27Kip1 accumulation in pre-osteoclast precursors. *J. Cell. Physiol.* **214**, 117–125 (2008).
35. M. Baud'huin *et al*., Osteoprotegerin: Multiple partners for multiple functions. *Cytokine Growth Factor Rev.* **24**, 401–409 (2013).
36. S. Taves *et al*., Hemophilia A and B mice, but not $VWF^{-/-}$ mice, display bone defects in congenital development and remodeling after injury. *Sci. Rep.* **9**, 14428 (2019).
37. L. J. Suva *et al*., Platelet dysfunction and a high bone mass phenotype in a murine model of platelet-type von Willebrand disease. *Am. J. Pathol.* **172**, 430–439 (2008).
38. G. Gerstner *et al*., Prevalence and risk factors associated with decreased bone mineral density in patients with haemophilia. *Haemophilia* **15**, 559–565 (2009).
39. S. S. Dufresne *et al*., Osteoprotegerin protects against muscular dystrophy. *Am. J. Pathol.* **185**, 920–926 (2015).
40. S. S. Dufresne *et al*., Genetic deletion of muscle RANK or selective inhibition of RANKL is not as effective as full-length OPG-fc in mitigating muscular dystrophy. *Acta Neuropathol. Commun.* **6**, 31 (2018).
41. K. K. Mak *et al*., Hedgehog signaling in mature osteoblasts regulates bone formation and resorption by controlling PTHrP and RANKL expression. *Dev. Cell* **14**, 674–688 (2008).
42. B. A. Alman, The role of hedgehog signalling in skeletal health and disease. *Nat. Rev. Rheumatol.* **11**, 552–560 (2015).
43. Y. Kawano, R. Kypta, Secreted antagonists of the Wnt signalling pathway. *J. Cell Sci.* **116**, 2627–2634 (2003).
44. M. A. Rudnicki, B. O. Williams, Wnt signaling in bone and muscle. *Bone* **80**, 60–66 (2015).
45. P. O. S. Kiper *et al*., Cortical-bone fragility–insights from sFRP4 deficiency in Pyle's disease. *N. Engl. J. Med.* **374**, 2553–2562 (2016).
46. R. Haraguchi *et al*., sFRP4-dependent Wnt signal modulation is critical for bone remodeling during postnatal development and age-related bone loss. *Sci. Rep.* **6**, 25198 (2016).
47. Y. Gong *et al*.; Osteoporosis-Pseudoglioma Syndrome Collaborative Group, LDL receptor-related protein 5 (LRP5) affects bone accrual and eye development. *Cell* **107**, 513–523 (2001).
48. M. Kato *et al*., Cbfa1-independent decrease in osteoblast proliferation, osteopenia, and persistent embryonic eye vascularization in mice deficient in Lrp5, a Wnt coreceptor. *J. Cell Biol.* **157**, 303–314 (2002).
49. J. von Maltzahn, C. F. Bentzinger, M. A. Rudnicki, Wnt7a-Fzd7 signalling directly activates the Akt/mTOR anabolic growth pathway in skeletal muscle. *Nat. Cell Biol.* **14**, 186–191 (2011).
50. L. I. Plotkin, A. L. Essex, H. M. Davis, RAGE signaling in skeletal biology. *Curr. Osteoporos. Rep.* **17**, 16–25 (2019).
51. Z. Zhou *et al*., Regulation of osteoclast function and bone mass by RAGE. *J. Exp. Med.* **203**, 1067–1080 (2006).
52. E. Galliera *et al*., Evaluation of circulating sRAGE in osteoporosis according to BMI, adipokines and fracture risk: A pilot observational study. *Immun. Ageing* **14**, 13 (2017).
53. N. M. Wolfman *et al*., Activation of latent myostatin by the BMP-1/tolloid family of metalloproteinases. *Proc. Natl. Acad. Sci. U.S.A.* **100**, 15842–15846 (2003).